VICTORIA UNIVERSITY
MELBOURNE AUSTRALIA

Effects of surface photocrosslinking on the properties of semi-refined carrageenan film

This is the Accepted version of the following publication

Effects of Surface Photocrosslinking on the Properties of Semi-Refined Carrageenan Film

Bakti B. Sedayu[1,2], Marlene J. Cran[1]*, Stephen W. Bigger[1]

[1]Institute for Sustainable Industries and Liveable Cities, Victoria University, PO Box 14428, Melbourne, 8001, Australia.

[2]Agency for Marine and Fisheries Research and Development, Republic of Indonesia. Jl. Pasir Putih II, Ancol Timur, Jakarta Utara 14430, Indonesia.

*Corresponding author: marlene.cran@vu.edu.au, Tel: +61 3 9919 7642

Abstract

The surface of semi-refined carrageenan (SRC) film samples were photocrosslinked with UV light using a solution of sodium benzoate as a photosensitizer. The surfaces were coated with a 6% (w/v) solution of the photosensitizer and exposed to the light source for 5, 10, 20 and 40 min. The effects of the surface crosslinking on the overall properties of the SRC films were investigated and related to the possible changes in the morphology of the substrate. The UV exposure and subsequent crosslinking were found to cause little color change in the films and increased the crystallinity as well as the thermal stability of the films. The mechanical properties were improved relative to the control sample with a *ca*. 36–55% range increase in the tensile strength observed, *ca*. 140–144% increase in the modulus but with a concomitant *ca*. 50-52% decrease in the elongation at break. The crosslinking decreased the inherent water content in the films by *ca*. 48–55% and decreased the water vapor transmission rate by *ca*. 10–21% relative to the control. The water sensitivity of the films, however, increased by *ca*. 18–44% and 9–23% for the water solubility and water uptake respectively, with decreases of *ca.* 18–22% in water contact angle. These changes were attributed to possible photodegradation products and the presence of residual photosensitizer that rendered the samples more hydrophilic. Under the conditions of the experiments, a UV exposure time of *ca*. 20 min was found to be optimal in enhancing the mechanical and water barrier properties. The results suggest photocrosslinking provides a promising step towards the production of a low-cost food packaging material from SRC raw materials.

Keywords: semi-refined carrageenan; sodium benzoate; photocrosslinking; UV irradiation; radar plots

1   Introduction

To address the negative environmental impacts caused by the use of petroleum-based plastics and satisfy increasing demands for alternative materials, the utilization of natural polymers for single-use packaging materials has gained increasing interest by researchers and industry. Although there are many natural resources that can be utilized for developing packaging materials, the majority are derived from terrestrial plants where intensive exploitation of these can introduce detrimental impacts on the environment. Some types of seaweeds can be farmed with minimal resources and polymers obtained from seaweeds are among the more advantageous alternatives for food packaging purposes (Sedayu, Cran, & Bigger, 2019; Shankar, Reddy, Rhim, & Kim, 2015).

38   Carrageenan is a linear, sulfated polysaccharide derived from red seaweed species, *Rhodophyta*, and
39   it has been used widely as a food additive among other uses (Necas & Bartosikova, 2013). Its strong
40   film-forming ability has further expanded the scope of carrageenan for use as a packaging film
41   material. Furthermore, in order to obtain less expensive carrageenan-based film, semi-refined
42   carrageenan (SRC) has also been used as the base material and has been reported to produce
43   comparable film properties to those made from refined carrageenan (Sedayu, Cran, & Bigger, 2020).
44   However, due to the inferior optical and mechanical properties of SRC film, it has been suggested the
45   material is more suitable for rigid-opaque packaging applications such as food containers, cups, etc.
46   (Sedayu, Cran, & Bigger, 2018) or food packaging films where high optical clarity is not required.

47   Regardless of the application, good mechanical strength and water resistance is necessary to prevent
48   packaging materials from physical deformation during handling and storage or when in contact with
49   food. These functions are also fundamental packaging requirements in order to preserve the packaged
50   food as well as maintain the food quality (Sothornvit & Rodsamran, 2008). Not unlike other bio-based
51   polymers, SRC films typically demonstrate inherently poor water vapor permeability and relatively
52   poor mechanical properties. Even though blending and reinforcement with hydrophobic or nano-sized
53   materials into the carrageenan polymer matrix has enhanced the film properties (Alves, Costa, &
54   Coelhoso, 2010; Kanmani & Rhim, 2014; Rhim & Wang, 2013; Sedayu, *et al.*, 2020), further
55   improvements may be possible by other means. Thus, alternative methods, or combinations of
56   methods, need to be investigated to optimally enhance the properties of SRC film.

57   One such method is crosslinking which results in the modification of the chemical structure of
58   biopolymer films. In principle, crosslinking can be described as the interconnection among the
59   polymer molecules within the matrix through some form of bonding such as covalent, ionic or
60   hydrogen bonding. This can subsequently change the network dynamics and molecular mobility within
61   the polymer, facilitate improved structural integrity of the film, and limit the interaction of the
62   polymer with water molecules (Detduangchan, Sridach, & Wittaya, 2014). For example, crosslinking
63   has been reported to successfully improve the mechanical properties as well as water vapor barrier of
64   cellulose/starch biocomposite films (Kumar & Singh, 2008).

65   In general, there are two techniques used to obtain a crosslinked polymer in bio-based films, namely
66   photo- and chemical crosslinking. Photocrosslinking involves the use of light where ultraviolet (UV)
67   radiation is most commonly used for this purpose as it is inexpensive, offers easy processing, and can
68   be applied to large-scale processing, particularly in the food industry (Zhou, *et al.*, 2009). In the case
69   of chemical crosslinking, the so-called bulk-crosslinking is the most common method as it can
70   effectively improve the functional properties of bio-based composites (Shahbazi, Ahmadi, Seif, &
71   Rajabzadeh, 2016). However, bulk-crosslinking is relatively expensive as it requires considerable
72   amounts of chemical crosslinking agents, and it also changes the overall chemical composition of the
73   biopolymer (Zhou, *et al.*, 2009).

74   Crosslinking that is confined to the surface of the material is an effective means of reducing the
75   amount of crosslinking agent required in the process whilst also maintaining the chemical composition
76   of the bulk polymer (Zhou, *et al.*, 2009). Surface photocrosslinking of biodegradable films such as
77   thermoplastic starch, polyvinyl alcohol and corn starch, has been shown to successfully reduce the
78   surface hydrophilicity of the films and increase their mechanical strength (Niazi & Broekhuis, 2015;
79   Villarruel, Giannuzzi, Rivero, & Pinotti, 2015; Zhou, Zhang, Ma, & Tong, 2008). Like carrageenan, these

80 materials have a large number of hydroxyl groups in their structure that are capable of undergoing
81 free-radical crosslinking reactions initiated by photosensitizers such as sodium benzoate (Bhat &
82 Karim, 2009). Moreover, due to its use in food preservation, sodium benzoate is reported to impart
83 desirable antimicrobial properties to material formulations used in food packaging (Birck*, et al.*, 2016;
84 Mondal*, et al.*, 2015).

85 In this study, surface photocrosslinking of SRC film formulations using sodium benzoate was
86 undertaken to assess the potential improvements to the barrier and mechanical properties. The
87 influence of the duration of exposure to UV irradiation on these properties was of particular interest
88 to optimize the treatment and obtain the most desirable properties.

89 **2   Materials and Methods**
90 **2.1   Materials**
91 Semi-refined carrageenan (E407a) derived from *Kappaphycus alvarezii* (formerly E*ucheuma cottonii*)
92 was obtained from W-Hydrocolloids Inc. (The Philippines) and its physical and chemical properties are
93 given elsewhere (Sedayu*, et al.*, 2020). Glycerol and sodium benzoate were used in the preparation of
94 films as the plasticizer and crosslinking agent respectively and were purchased from Sigma-Aldrich
95 (Sydney, Australia). Saturated $Mg(NO_3)_2$ solution was purchased from Ajax Finechem (Sydney,
96 Australia) and Milli-Q water was used as the solvent for the film preparations.

97 **2.2   Film Preparation**
98 The SRC film samples were prepared according to a procedure described in a previous study (Sedayu*,
99 et al.*, 2018). Briefly, a 2% (w/w) aqueous solution of SRC was stirred at a constant temperature of
100 90°C for 30 min followed by the addition of glycerol (40% (w/w) relative to SRC). Aliquots of 40 mL of
101 the solution were poured onto an acrylic tray (200 × 150 × 3 mm) and allowed to dry for 36 h at
102 ambient temperature (*ca.* 22 °C).

103 Aqueous sodium benzoate (30 mL of 6% (w/v) solution) was poured evenly onto the upper surface of
104 the dried SRC films where it remained for 2 min before the excess solution was drained away, and the
105 films left to dry for 24 h at 22 °C. After that, the samples of film were exposed to UV light in a laminar
106 flow cabinet (Laftech, Australia) equipped with a Philips UV light TUV 30W/G30T8 (USA) for different
107 times (0, 5, 10, 20 and 40 min). The surface of the films treated with sodium benzoate were directly
108 exposed to the UV source that had a total photon count intensity (integrated between 250 and 400
109 nm) of 1.4×10^{-6} mol m^{-2} s^{-1}. A sample of SRC film that had not been coated with sodium benzoate or
110 exposed to UV light was used as the control in each of the experiments.

111 The average film thickness of each sample was obtained from at least 3 measurements at random
112 locations on the film and was measured using a digital micrometer (Schut IP54, The Netherlands) with
113 an accuracy 0.001 mm. Prior to testing, the films were cut into specimens of the following dimensions:
114 20 × 20 mm for the water content and water solubility measurements, 50 × 25 mm for water uptake
115 measurements, 100 × 15 mm for mechanical property measurements, and 11.3 mm diameter discs
116 for the water vapor permeability (WVP) measurements. Prior to testing, all samples were
117 preconditioned at 53% RH in a desiccator containing saturated $Mg(NO_3)_2$ solution (Ajax FineChem,
118 Australia) and stored in the dark for at least 24 h.

2.3 Color Properties

The lightness ($L*$), redness/greenness ($a*$), and yellowness/blueness ($b*$) color parameters of the film samples were measured using a chroma-meter (Konica Minolta CR-400, Japan). At least three data points were recorded for each film and samples were tested in triplicate using a standard white tile ($L*$ = 97.39, $a*$ = 0.03 and $b*$ = 1.77) as the base for the films and for calibration of the chroma-meter.

2.4 Water Sensitivity and Water Barrier Properties

The water content was measured by drying 2 × 2 cm film samples in an air-circulating oven set at 105 °C, until a constant dry weight of each sample was obtained. The percentage water content was calculated from the difference between the mass of the film before and after heating.

Water uptake of the films was measured using film samples of 5 × 2.5 cm that were previously dried in an air-circulating oven at 60 °C for 48 h. The samples were accurately weighed before being placed in a desiccator maintained at 98% RH using a saturated solution of KNO_3. The desiccator was incubated for 24 h at 25 °C and the percentage water uptake was calculated from the increase in film mass.

Water solubility was measured using square samples of film (*ca.* 12.7 mm^2) which were first dried for 24 h at 105 °C in an air-circulating oven (Rhim*, et al.*, 2013). Samples were then inserted in 50 mL centrifuge tubes containing 30 mL of water before the tubes were capped and placed in a shaker water bath (Ratek SWB20D, Australia) for 30 min at 25 °C with constant, gentle shaking. The undissolved pieces of film were removed from the tube and gently dried using absorbent tissue and were subsequently dried for 24 h at 105 °C in an air-circulating oven. The percentage water solubility was calculated from the difference between the amount of film remaining and the initial mass.

A drop shape analyser (Kruss DSA30S, Germany) was used to measure the contact angle of film samples that were adhered onto glass slides. A micro-syringe was used to place a 4 μL water droplet onto the surface of the film and the angle between the horizontal baseline of the water droplet and the droplet boundary tangent was measured using Advance 1.6.1.0 software. A minimum of ten measurements were performed on each film sample to obtain the average.

The water vapor permeability (WVP) was measured by sealing a circular section of film on the lid of a permeation cup containing silica gel to maintain 0% RH inside the cup (Sobral, Menegalli, Hubinger, & Roques, 2001). The prepared cups were placed on a tray in a desiccator containing water in the base to maintain 100% RH, ensuring that the cups were located above the water. The desiccator was maintained at 22 °C and the mass of each cup was measured daily for 7 days. The WVP was calculated using equation (1):

$$WVP = \frac{x}{\Delta P} \times \frac{w}{tA} \qquad (1)$$

where x is the film thickness (mm), ΔP is the difference in the partial pressures (Pa) of water vapor across the film, w is the mass (m) of the sample cup at time t (h), and A is the area of the film (cm^2).

2.5 Thermal Properties

Thermogravimetric (TG) analysis of the film samples was investigated using a Mettler-Toledo TGA/DSC1 thermal analyzer (Mettler Toledo, Schwarzenbach, Switzerland). Samples of 8-12 mg were placed in alumina crucibles and were heated from 30 to 400 °C at a heating rate of 10 °C min^{-1} using

158 nitrogen purge gas at a flow rate of 20 mL min^{-1}. Differential scanning calorimetry (DSC) analyses were
159 performed using a Mettler Toledo DSC1 instrument (Mettler Toledo, Schwarzenbach, Switzerland).
160 Samples of 5-10 mg were crimped inside 40 μL aluminum crucibles and were heated from 50 to 320
161 °C at 10 °C min^{-1} using nitrogen purge gas at a flow rate of 20 mL min^{-1}. Both the TG and DSC data were
162 analyzed using Mettler Toledo STAR^{e} V11 software.

163 **2.6   Mechanical Properties**
164 The tensile strength (TS), Young's modulus (YM) and elongation at break (EB) were determined in
165 accordance with ASTM D882 (2012) using an Instron Universal Testing Machine (Model 4301) fitted
166 with a 5 kN load cell. An initial gauge length of 50 mm and a cross-head speed of 10 mm min^{-1} was
167 used for each sample and the resulting stress-strain curves were evaluated using BlueHill Series IX
168 software. A minimum of eight strips of film (10 × 1.5 cm) were measured for each sample to obtain an
169 average value for each of the measured properties.

170 **2.7   Structural Properties**
171 Changes in the crystallinity of the film samples were assessed by X-ray diffraction (XRD) measurements
172 using a Rigaku Miniflex 600 diffractometer operating at 40 kV and 20 mA using a Cu Kα (λ = 0.154 nm)
173 radiation source without the use of a monochromator over a 2θ range of 5–40°. Fourier transform
174 infrared (FTIR) spectra of the film samples were obtained using a Perkin-Elmer Frontier FTIR
175 spectrophotometer (PerkinElmer, Inc., Waltham, USA). Film samples were clamped onto the diamond
176 crystal attenuated total reflectance accessory and an average of 64 scans at 4 cm^{-1} resolution were
177 obtained over the range 4000-600 cm^{-1}. Data analysis was performed using the Perkin-Elmer Spectrum
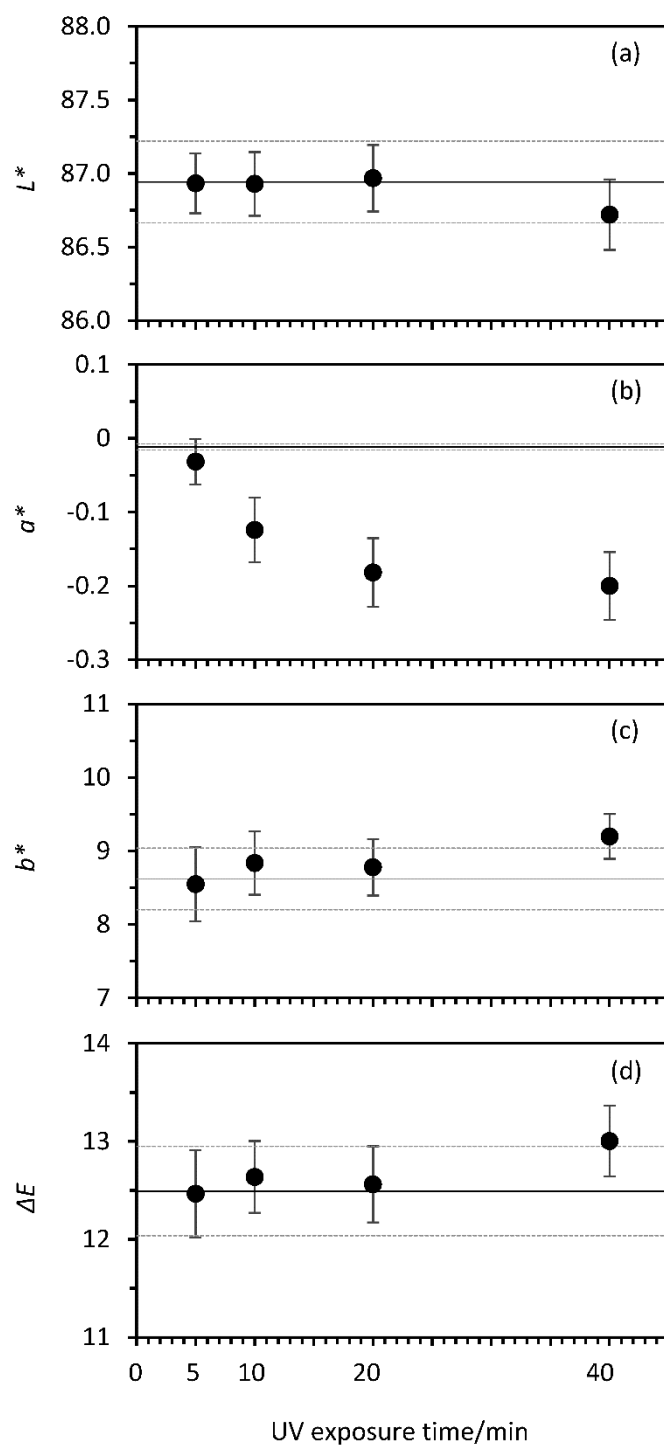178 10^{TM} software.

179 **2.8   Statistical Analysis**
180 All collected experimental data were processed by a one-way analysis of variance using the SPSS
181 statistics software program (SPSS Statistical Software Inc., USA), and the significant differences among
182 the samples further evaluated with a Duncan test set at $p \leq 0.05$.

183 **3   Results and Discussion**
184 **3.1   Surface Color**
185 The color parameters pertaining to the surfaces of the SRC films at different times of exposure to the
186 UV source are presented in Figure 1 with the statistical analysis provided in the Supplementary
187 Material (Table S1). Upon UV exposure, all SRC films retained their yellowish translucent appearance
188 with the lightness (L^{*}) and overall colour difference (ΔE) remaining relatively unchanged with respect
189 to the control film. A significant reduction in the redness (a^{*}) is observed which is possibly
190 compensated for by a slight increase in the yellowness (b^{*}) with the longer UV irradiation times,
191 particularly for exposure times greater than 10 min. These colour changes may indicate that some
192 photodegradation of the film has occurred under prolonged exposure to the UV source which is
193 consistent with reports of other bio-based films such as in soy protein (Gennadios, Rhim, Handa,
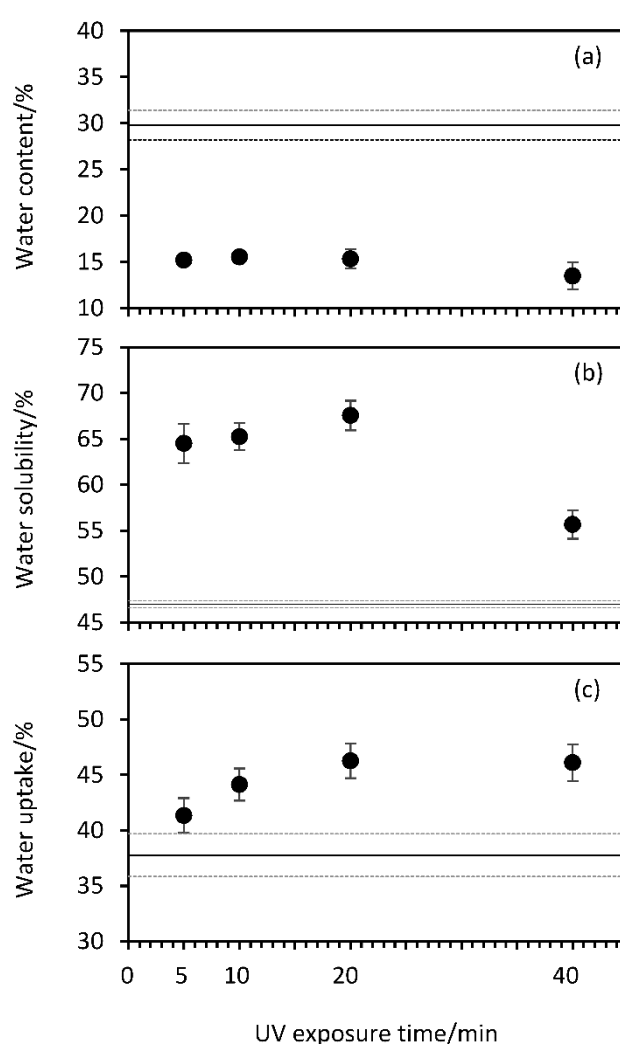194 Weller, & Hanna, 1998) and gelatine/chitosan films (Salami, Rezaee, Askari, & Emam Djomeh, 2020).

195

Figure 1. Color parameters of the UV-crosslinked SRC films at different times of UV exposure: (a) L^*, (b) a^*, (c) b^*, and (d) ΔE. The horizontal lines represent the mean value of the control film (solid) ± 1 SD (dashed).

3.2   Water Sensitivity and Barrier Properties

Figure 2 shows the water content, water solubility and water uptake data for the SRC control film and those films treated by UV crosslinking. The statistical analysis is provided in the Supplementary Material (Table S2). A significant decrease of ca. 50% in the water content of the SRC samples is observed for the crosslinked samples in comparison to the control film. This is a result of the reduced

204 number of hydroxyl groups present in the crosslinked polymer that are available to interact with and
205 retain water molecules as well as the increased crystallinity (see Section 3.5 below) that reduces the
206 extent of the amorphous regions where water can be accommodated. The water solubility values are
207 *ca*. 35% higher than the control which is an unexpected result. Nonetheless, the value seems to be
208 decreased at 40 min exposure suggesting a possible downward trend in the value at much longer
209 exposure times. Similarly, the water uptake is unexpectedly higher than the control, showing an
210 upward trend with the time of UV exposure and a maximum value of *ca*. 46% at 20 min (i.e. about
211 22% higher than the control). This may be explained by the photodegradation of the polymer during
212 exposure to the UV source during which pores and microcracks in the polymer structure may be
213 created (Zhou*, et al.*, 2008) that consequently deteriorate the water sensitivity properties of the film.
214 Evidence of photodegradation can be seen in the results of the surface colour measurements as shown
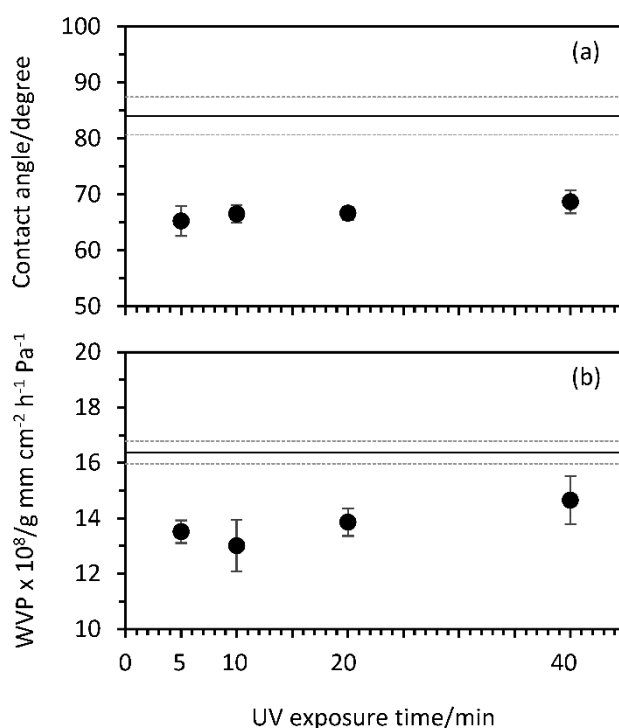215 in Figure 1.

216

217 **Figure 2**. Plots of: (a) water content, (b) water solubility and (c) water uptake of the UV-crosslinked
218 SRC films at different times of UV exposure. The horizontal lines represent the mean value of the
219 control film (solid) ± 1 SD (dashed).

220 Figure 3 shows the WVP and contact angle as a function of time of exposure to the UV source. The
221 statistical analysis is provided in the Supplementary Material (Table S2). In both cases, the values
222 obtained for the films subjected to UV treatment are consistently lower than that of the control SRC

film. The contact angle results are consistent with the water solubility and water uptake results which suggests the crosslinked samples have a higher affinity for water than the control with the contact angles being *ca*. 21% lower than the control. The WVP values are favorable in comparison with the control as these are on average *ca*. 16% lower than the control with an apparent minimum at an exposure time of 10 min. Similar enhancements in water vapor barrier properties by crosslinking have also been reported in the case of starch and chitosan films (Delville, Joly, Dole, & Bliard, 2002; Kumar, *et al.*, 2008; Liang, Wang, & Chen, 2019). There is an overall upward trend in the WVP values with increasing time of exposure which is consistent with the notion that photodegradation at higher levels of exposure may lead to pores, microcracks, etc., that render the material more permeable to water. Nonetheless, the overall decrease in the WVP through the film that has occurred due to crosslinking can be explained by: (i) the decrease in hydroxyl groups (see Section 3.5 below) that are capable of facilitating the transfer of water molecules (Müller, Laurindo, & Yamashita, 2011), (ii) the formation of intermolecular bridges (Zhou, *et al.*, 2008) within the matrix and (iii) increased crystallinity (see Section 3.5 below) resulting in fewer amorphous regions in the polymer and thereby increasing the tortuosity within the polymer matrix (Shahbazi, *et al.*, 2016).
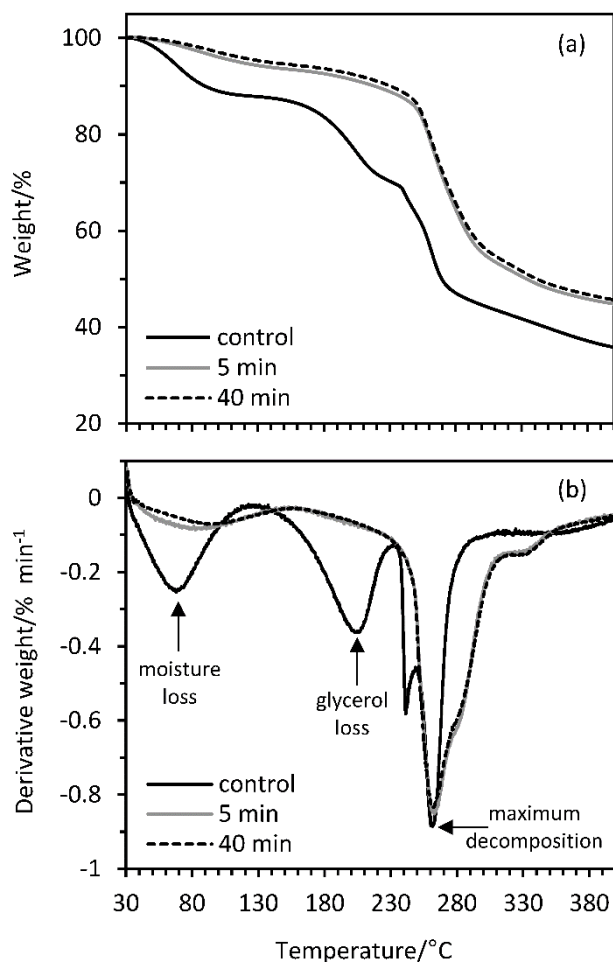

Figure 3. Plots of: (a) contact angle and (b) WVP of the UV-crosslinked SRC films at different times of UV exposure. The horizontal lines represent the mean value of the control film (solid) ± 1 SD (dashed).

Collectively, the water solubility, water uptake and contact angle results all suggest that crosslinking has sensitized the material to water. This apparent increase in the water sensitivity of the SRC may be due to the presence of residual sodium benzoate present on or near the surface of the crosslinked SRC films. Sodium benzoate is a hygroscopic compound that is readily soluble in water (solubility 62.7 g per 100 mL at 20 °C) and so the presence of any residual sodium benzoate in the sample will render it more hygroscopic which, in turn, enables it to absorb more water.

3.3 Thermal Properties

The thermal degradation behavior of crosslinked films in comparison with the control SRC film was evaluated by TG analysis. The results shown in Figure 4 present the normalized mass loss and derivative mass loss (dTG) as a function of temperature of the control sample and those exposed to the UV source for 5 and 40 min. The TGA profile of the control sample is markedly different to those of the crosslinked samples which, in turn, are almost superimposable on one another with only slight differences able to be seen in the overlaid TG profiles. The complete set of TG data are presented in the Supplementary Material (Figure S1). The initial mass loss that occurs at *ca*. 100 °C in the control sample is attributed to the loss of water in the sample. The corresponding mass losses in the crosslinked samples are significantly less suggesting that these samples have an inherently lower water content than the control. This result is also consistent with the previous water content analysis (see Figure 2) in so far as crosslinking reduces the inherent water content of SRC with an apparent downward trend in the water content with increasing time of UV exposure. However, the average water content measured by the TG mass loss at 105 °C is *ca*. 11% and 3% for the control and averaged crosslinked films respectively whereas that measured gravimetrically is *ca*. 30% and 15% for the respective control and averaged crosslinked films.

Figure 4. Plots of: (a) normalized mass loss and (b) derivative mass loss as a function of temperature for the SRC control film and SRC films crosslinked with sodium benzoate for 5 and 40 min UV exposure times. Samples were heated from 30 to 400 °C at a heating rate of 10 °C min^{-1} under a nitrogen atmosphere (20 mL min^{-1} flow rate).

9

269 The second stage in the TG decomposition of the control sample that is clearly visible between *ca*.
270 170–225 °C is attributed to the volatilization of plasticizer (glycerol) from the polymer matrix (Rhim,
271 2013). Interestingly, this second stage of decomposition appears to be almost absent in the case of
272 the crosslinked films, an observation that is supported more readily by the dTG plot of the data shown
273 also in Figure 4. It is possible that the volatilization of the plasticizer in the crosslinked films may be
274 shifted to higher temperatures due to the egress of the plasticizer having been inhibited by the
275 crosslinking. In particular, such delayed volatilization may be ascribed to stronger hydrogen bonding
276 and covalent bonding near or at the surface of the polymer brought about by the crosslinking (Zain,
277 Wahab, & Ismail, 2018). As a result, the plasticizer may have been degraded along with the
278 carrageenan at a later stage in the profile. The third stage shown in the TG profiles corresponds to the
279 thermal degradation of the carrageenan polymer and occurs within the temperature range of *ca*.
280 240−275 °C for the control SRC film and *ca*. 240−300 °C for the crosslinked films. The slightly broader
281 temperature range observed in the case of the crosslinked films might also be explained similarly by
282 there being a stronger polymer chain network, as already suggested.
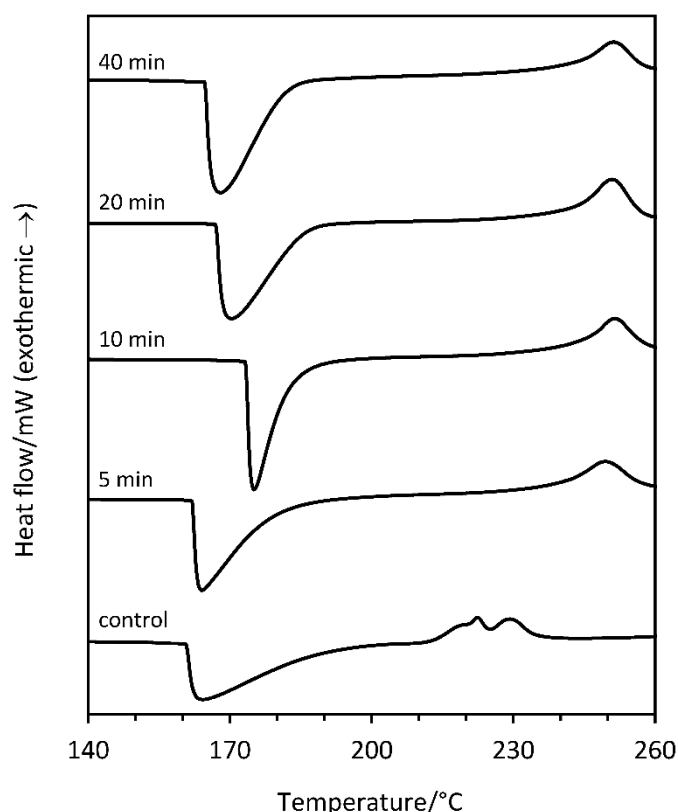
283 Table 1 lists the numerical data extracted from the TG thermograms shown in Figure 4. These data
284 indicate the crosslinking slightly shifted the onset temperature of the decomposition of carrageenan
285 from *ca*. 249 °C to an average of *ca*. 253 °C and slightly shifted the temperature at which the maximum
286 rate of decomposition occurred from *ca*. 263 °C to an average of *ca*. 266 °C thereby consistent with
287 there being enhanced thermal stability in the crosslinked films. At UV exposure times longer than 5
288 min, however, there appears to be no further increase in the thermal stability of the SRC film. The
289 mass loss data at 100 °C suggest that the inherent water content in the crosslinked films is on average
290 *ca*. 69% less than the control and that there is a steadily decreasing trend in the water content with
291 an increasing period of UV exposure. Although such a trend is not observed in the data for 275 °C and
292 400 °C, the average mass loss of the crosslinked samples at 275 °C is *ca*. 41% less than the control,
293 further confirming the notion that the crosslinking has thermally stabilized the SRC to some extent.
294 Similarly, at the extreme temperature of 400 °C, the average mass loss of the samples is *ca*. 15% less
295 than the control thereby leading to the same conclusion.

296 **Table 1**. Decomposition temperatures and mass loss data of SRC films at crosslinked with different
297 times of UV exposure.

UV exposure time/min	Decomposition temperatures/°C		Mass loss/%		
	T_{onset}	$T_{max.}$	100 °C	275 °C	400 °C
Control	249	263	11.1	54.3	64.2
5	253	266	3.94	32.3	55.2
10	254	266	3.39	31.1	53.9
20	253	267	3.25	32.7	55.9
40	253	265	2.95	31.1	54.3
Average	253	266	3.38	31.8	54.7
Difference			69%	41%	15%

298

299 The effects of crosslinking on the thermal properties of the SRC films are also depicted in the DSC
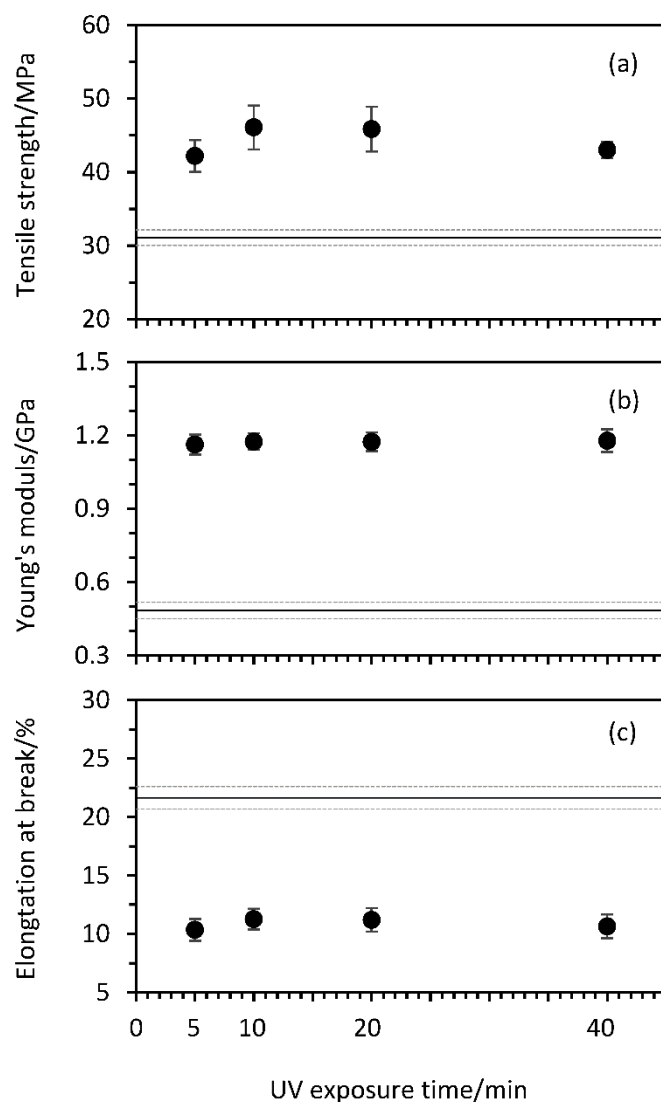300 thermograms shown in Figure 5 where the broad, endothermic peak assigned to the glass transition

301 temperature (T_g) of the SRC is observed to shift from *ca*. 163 °C to *ca*. 174° in the case of the sample
302 crosslinked at 10 min exposure to the UV source. The downward shift in the T_g values for samples
303 exposed to the UV source for 20 and 40 min may be due to photodecomposition having occurred in
304 these samples. The latter is also supported by the significant shift in the exothermic peaks towards
305 higher temperatures (see Figure 4) that are attributed to the decomposition of the SRC film.

306

307 **Figure 5**. DSC thermograms of the SRC control film and SRC films crosslinked at different times of UV
308 exposure. Samples were heated under nitrogen (flow rate 20 mL min^{-1}) from 50 to 320 °C at a heating
309 rate of 10 °C min^{-1}.

310

311 **3.4   Mechanical Properties**
312 The TS, YM and EB results for the control SRC film and those subjected to UV crosslinking are shown
313 in Figure 6 with the statistical analysis provided in the Supplementary Material (Table S3). The TS
314 values of the crosslinked films were on average *ca*. 42% greater than the control and these values
315 increased with an increasing time of exposure to the UV source. A *ca*. 55% increase in TS compared to
316 the control was attained at 20 min after which the TS dropped significantly at 40 min of UV exposure
317 presumably due to degradation. The YM values were on average *ca*. 142% greater than the control
318 with no significant changes with increasing UV exposure time. As expected, the EB values of the
319 crosslinked films were considerably lower than that of the control (on average *ca*. 50% lower than the
320 control) and these values appear to follow a similar trend to the TS values in that a maximum was
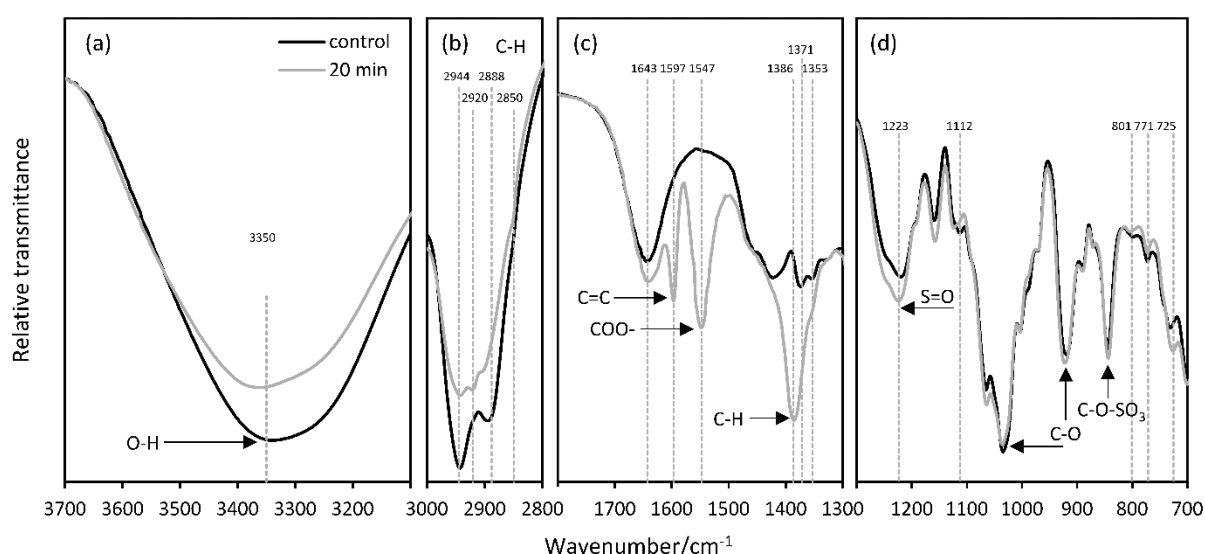321 reached at 20 min UV exposure.

11

322

Figure 6. Plots of: (a) tensile strength, (b) Young's modulus, and (c) elongation at break of the crosslinked SRC films at different times of UV exposure. The horizontal lines represent the mean value of the control film (solid) ± 1 SD (dashed).

The observed changes to the tensile properties upon crosslinking are due to intermolecular bridges formed among the carrageenan chains in the matrix which contribute to a prominent, firmer and stiffer structure (Shahbazi, *et al.*, 2016). The increase in the TS corresponds to an increased level of crosslinking within the SRC matrix which, in turn, is determined by the duration of exposure to the UV source (Decker & Moussa, 1988). However, a sufficiently long period of UV exposure (or a higher UV intensity) may also promote rapid chain cleavage of the SRC that may equally degrade the polymer structure (Khan, Bhattacharia, Kader, & Bahari, 2006), evidence of which can be seen in the color parameters (Figure 1) corresponding to the higher levels of UV exposure. Hence, there is a maximum time for which samples should be exposed to the UV source in order to optimize the mechanical properties such as the TS that are imparted by crosslinking. The results in Figure 6 suggest that such a time is *ca*. 20 min for the SRC films under the conditions used in this study.

3.5 Chemical Structure and Crystallinity

Fourier transform infrared spectroscopy was used to observe any noticeable changes in the chemical structure of the SRC films as a result of the UV crosslinking. Shown in Figure 7 is the FTIR spectra of the control SRC film derived from *K. alvarezii* extracted carrageenan, the main industrial source of κ-carrageenan, which shows strong absorption bands in the region of 930 cm^{-1} (CO of 3,6-anhydrogalactose) and in the 845 cm^{-1} region (CO-SO$_4$ in C$_4$ of galactose), which are both typical of the presence of κ-carrageenan. The spectrum also exhibits reduced absorbance in the region 805 cm^{-1} (CO-SO$_4$ in C$_2$ of anhydrogalactose), which indicates the presence of small quantities of ι-carrageenan. The FTIR spectrum of the SRC film exposed to the UV light for 20 min is also shown in Figure 7 for comparison. The spectra of all UV-exposed samples were almost identical, so only one example film is presented for comparison to the control. The complete set of spectra for all film samples and that of sodium benzoate are presented in the Supplementary Material (Figure S2).
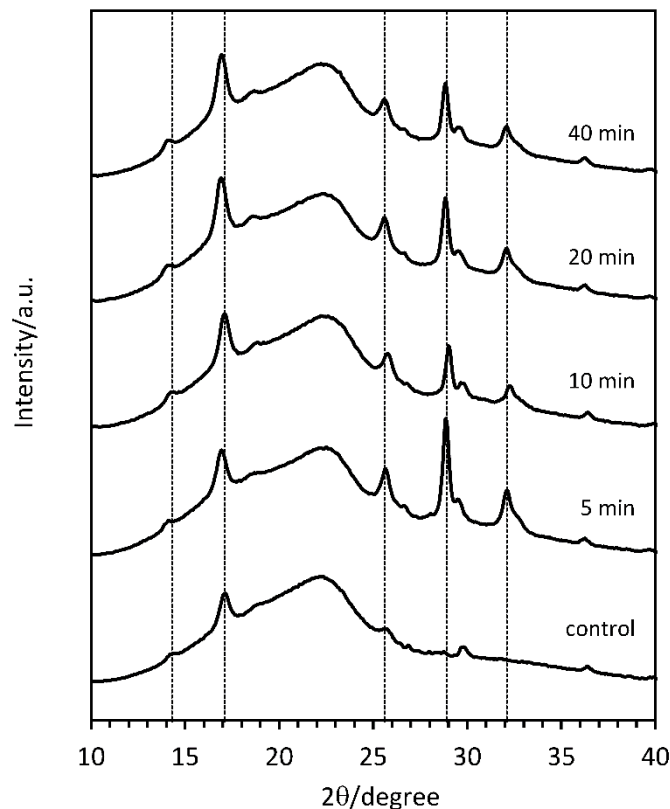

Figure 7. FTIR spectra of the control SRC film and SRC film crosslinked at 20 min exposure to UV irradiation over the wavenumber ranges: (a) 3700-3000 cm^{-1}, (b) 3000-2800 cm^{-1}, (c) 1800-1300 cm^{-1}, and (d) 1300-700 cm^{-1}. Spectra are the average of 64 scans.

The crosslinking resulted in a less intense vibrational stretching band at 3700–3000 cm^{-1} that corresponds to free, inter- and intra-hydroxyl group bonding as well as a slightly less intense band at 2990–2830 cm^{-1} attributed to the alkyl C−H stretch associated with aliphatic chains of the SRC polymer (Karbowiak, Ferret, Debeaufort, Voilley, & Cayot, 2011). Additional peaks are also identified in the crosslinked SRC film at 1597, 1548 and 1385 cm^{-1} that presumably originate from the sodium benzoate (see Figure S2 in Supplementary Material). These are attributed respectively to the C=C bonds, asymmetric carboxylate anion (COO$^-$), and C−H bonds of the benzoate ring (Miranda, Goncalves, & Amorim, 2001). The remaining vibrational stretches observed at wavenumbers 1225, 1035, 922 and 840 cm^{-1} are respectively attributed to the S=O bonds of sulfate esters, C−O bonds of the glycosidic linkage of 3,6-anhydro-D-galactose, the C−O bond of 3,6-anhydro-D-galactose, and the C−O−SO$_3$ bonds of D-galactose-4-sulfate all of which represent the typical vibrational stretching found in SRC film (Sedayu, *et al.*, 2018). In general, there are no significant changes in the sulfate bonds representing these inherent SRC structures.
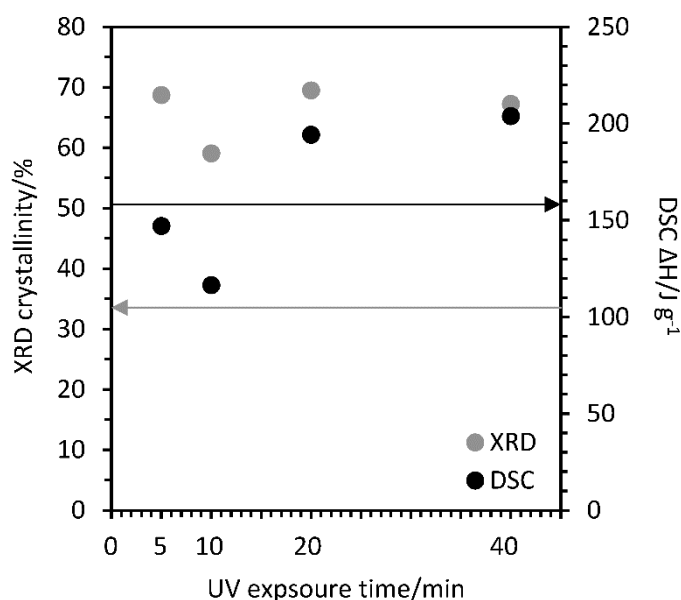
13

The significant reduction in the hydroxyl band at 3700–3000 cm^{-1} that occurs upon UV treatment of the SRC confirms the notion that crosslinking occurs mainly through hydroxyl groups (Farhan & Hani, 2017) and this finding is consistent with the reduced water content observed in the gravimetric and TG experiments shown in Figure 2 and Figure 4 respectively. Similar results have been observed in other comparable polymer systems that have been subjected to UV crosslinking (Bhat, *et al.*, 2009; Sonker, Rathore, Nagarale, & Verma, 2018). In the case of sodium benzoate, the production of reactive benzoate free radicals by UV radiation induces the abstraction of tertiary hydrogen atoms of the SRC polymer rendering a polymeric radical (Zain, *et al.*, 2018) that may further interact with hydroxyl groups within the SRC structure, thus facilitating the crosslinking of the carrageenan polymer chains. Moreover, the reactions of free radicals produced from the sodium benzoate may also contribute to a decrease in the number of C−H bonds of alkanes from aliphatic chains and an increase in the number of the C−O bonds of the glycosidic linkage of 3,6-anhydro-D-galactose from the original SRC polymer.

Shown in Figure 8 are the XRD spectra that were obtained to observe any changes to the crystallinity resuting from crosslinking. The control SRC film has a semi-crystaline structure with a broad shoulder at the band between 2θ = 17.8–24.8° due to the amorphous regions along with crystalline peaks identified at 2θ = 14.3°, 17.1°, 25.6° and 29.8°, which are consistent with peaks observed in the diffraction spectrum of the type I cellulose (El Achaby, Kassab, Aboulkas, Gaillard, & Barakat, 2018). The peak at 36.4° corresponds to minerals or unknown impurities typically found in seaweed (Corvaglia, Rodriguez, Bardi, Torres, & Lopez, 2016; El Achaby, *et al.*, 2018). Relative to the control sample, the intensity of the peaks at 2θ = 14.3°, 17.2° and 25.6° increased with the longer exposure times and additional, prominent, sharp diffraction peaks also appeared at 2θ = 28.9° and 32.1°.

Figure 8. XRD spectra of the SRC control film and SRC films crosslinked with UV irradiation at different times of exposure. The spectra were recorded using Cu Kα radiation (λ = 0.154 nm) at 40 kV and 20 mA.

390 Figure 9 shows a comparison of the percentage crystallinity of the films measured by XRD and the
391 apparent crystallinity measured by DSC obtained by calculating the ΔH value of the main SRC
392 crystalline peak. The XRD data show that exposure to the light source for 5 min resulted in a doubling
393 of the crystallinity relative to that of the control film. Increasing the time of exposure to 10 min also
394 resulted in a higher crystallinity than that of the control but was lower than that observed at 5 min.
395 Further exposure of the samples to the UV source maintained the crystallinity at a similar level to that
396 obtained for 5 min exposure. This possibly confirms that the crosslinking is confined primarily to the
397 surface regions of the samples and the resulting increase in the crystallinity of the SRC film has
398 occurred due to an increase in the macromolecular chain network (Zhou*, et al.*, 2009). The increased
399 crystallinity observed upon crosslinking is also consistent with observations made on crosslinked
400 carboxymethyl cellulose film (Shahbazi*, et al.*, 2016). with regard to the present study, this result may
401 also explain the overall increased thermal stability obtained by the TG analysis (see Figure 4) as well
402 as the increase in the TS and YM (see Figure 6). The overall trends in the ΔH values obtained from the
403 DSC data are similar to that obtained from the XRD data although in this case, both the 5 min and 10
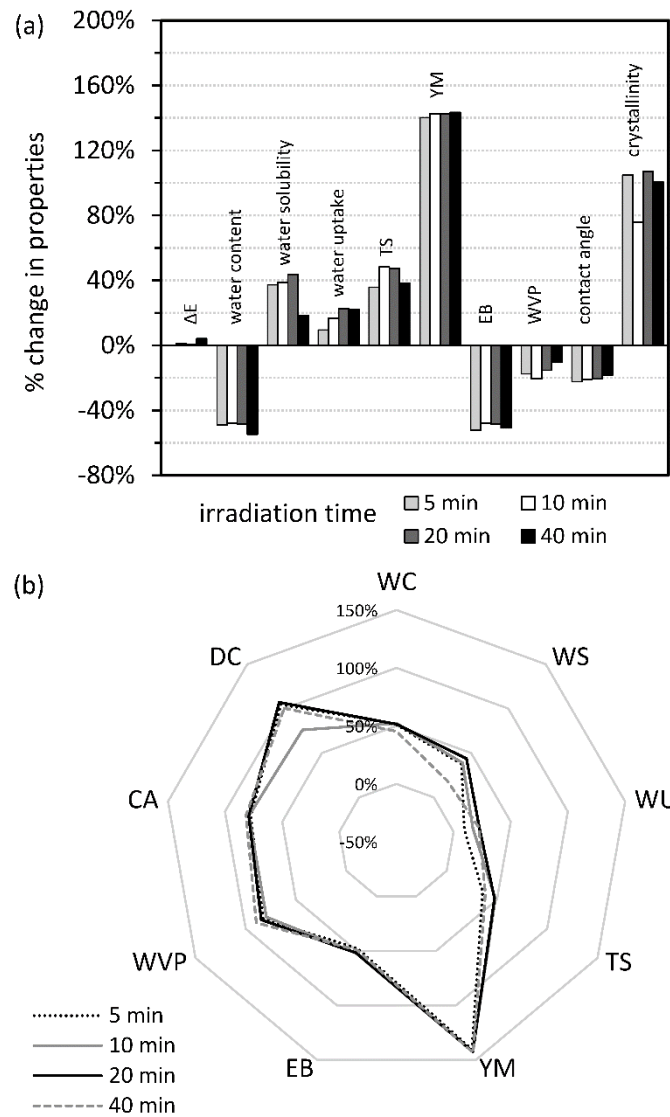404 min exposures resulted in values lower than the control film.

405

Figure 9. Plots of percentage crystallinity obtained from the XRD data and ΔH values obtained from
407 DSC data for SRC films crosslinked with UV irradiation for different exposure times. The horizontal
408 lines with arrows represent the values of the SRC control films.

409 **3.6 Optimization of UV Irradiation Time**
410 A semi-quantitative approach was used to collate the key properties of the film as a function of UV
411 irradiation time in order to ascertain the overall optimum treatment. The data were first normalized
412 to that of the untreated film and Figure 10(a) shows the percentage difference between each property
413 measurement and the control. The results show that the YM in particular is increased with UV
414 treatment and this is consistent with the concomitant increase in the percentage crystallinity. In some
415 cases, the differences are negative indicating a reduction in the measured property over the control,
416 however, these values represent an improvement in the measured property with the exception of the
417 EB values which decreased. Radar plots were constructed using normalized data where the negative
418 values representing an improved property were made positive such that an improvement in the

15

overall properties of the film is indicated by increasing area of the resulting polygon (Cran & Bigger, 2005; Kuorwel, Cran, Sonneveld, Miltz, & Bigger, 2014) as shown in Figure 10(b). The plot suggests that the 20 min irradiation time results in the film with the best overall properties.
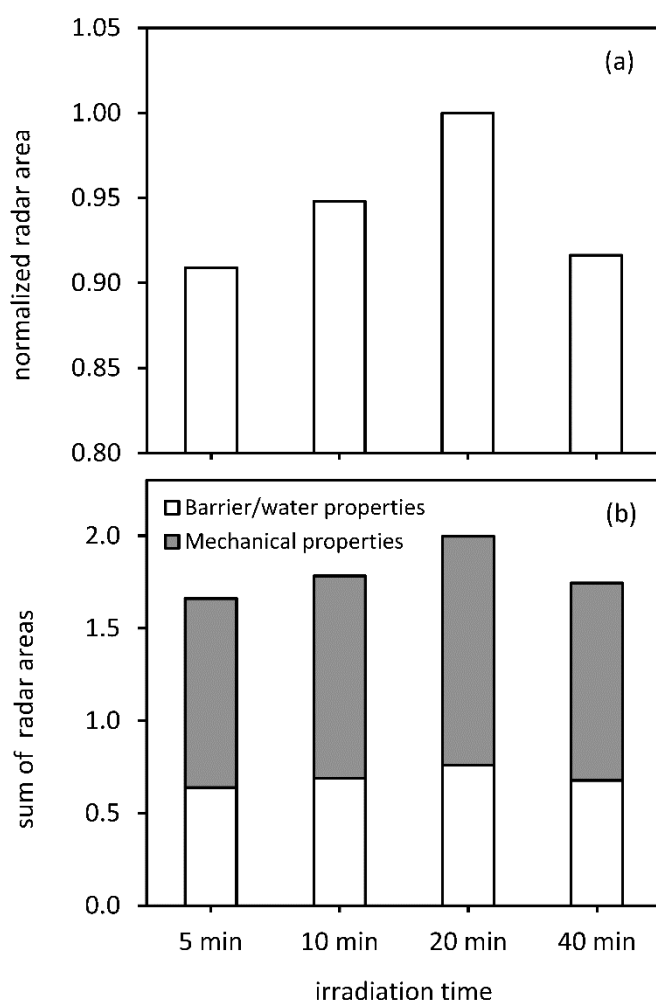

Figure 10. Optimization of UV treatment: (a) histogram of the percentage change in properties at different times of UV exposure and (b) radar plots of the percentage change in properties. Note: WC = water content, WS = water solubility, WU = water uptake, TS = tensile strength, YM = Young's modulus, EB = elongation at break, WVP = water vapor permeability, CA = contact angle, and DC = degree of crystallinity.

The greater the total area of the resulting polygon obtained from the radar plot, the better the overall properties of the film tested. The total area of the polygon (A_T) is the sum of the areas of the triangular segments (Cran, *et al.*, 2005) which can be calculated using equation (2):

$$A_T = \sum_{i=1}^{n-1} \frac{1}{2} r_i \, r_{i+1} \, sin(\frac{2\pi}{n}) + \frac{1}{2} r_{n-1} r_1 \, sin(\frac{2\pi}{n}) \qquad (2)$$

where *i* is the segment of ordinate *r* and *n* is the total number of segments of the polygon.

16

433　Figure 11(a) shows a plot of the normalized sum of areas of the polygons shown in Figure 10(b) and
434　as previously indicated, UV irradiation for 20 min clearly results in the optimum overall film properties.
435　Shown in Figure 11(b) is the sum of the radar areas on the basis of the property type and it is evident
436　that the mechanical properties contribute to the total polygon area to the greatest extent.

438　**Figure 11**. Histograms of: (a) normalized radar area and (b) sum of the radar plot areas based on
439　barrier/water and mechanical properties of the samples at different times of UV exposure.

440　**4　Conclusions**
441　This study has demonstrated the potential to enhance the mechanical and barrier properties of SRC
442　films by photocrosslinking these with a view to producing food packaging films with enhanced
443　properties from renewable resources and which have little impact on the land environment. The
444　photocrosslinking of SRC film at or near the surface using sodium benzoate and UV irradiation appears
445　to have only a slight effect on the color of the film with some evidence of photodegradation at longer
446　exposure times. Treatment with UV irradiation decrease the number of hydroxyl groups and increases
447　the crystallinity of the SRC polymer due to the crosslinking and other reactions initiated by the
448　photosensitizer. The morphological and chemical changes brought about by crosslinking, particularly
449　at the lower levels of UV exposure, impart a slight thermal stability to the bulk of the material but
450　perhaps more importantly, enhance the tensile strength and modulus but with an expected
451　concomitant decrease in the elongation at break. The crosslinking also decreases the transmission of

17

452 water through the film as well as decreases the inherent water content. However, it appears that the
453 presence of residual photosensitizer in SRC film increases the overall water sensitivity. Based on the
454 semi-quantitative analysis using radar plot area calculations, an optimum irradiation time of 20 min
455 resulted in films with the best overall properties.

Declaration of competing interest

457 The authors declare no conflict of interest.

References

459 Alves, V. D., Costa, N., & Coelhoso, I. M. (2010). Barrier properties of biodegradable composite films
460   based on kappa-carrageenan/pectin blends and mica flakes. *Carbohydrate Polymers, 79*(2),
461   pp. 269-276. https://doi.org/10.1016/j.carbpol.2009.08.002.

462 ASTM D882-12 (2012). Standard Test Method for Tensile Properties of Thin Plastic Sheeting. ASTM
463   International, West Conshohocken, PA, www.astm.org.

464 Bhat, R., & Karim, A. A. (2009). Impact of radiation processing on starch. *Comprehensive Reviews in
465   Food Science and Food Safety, 8*(2), pp. 44-58. https://doi.org/10.1111/j.1541-
466   4337.2008.00066.x.

467 Birck, C., Degoutin, S., Maton, M., Neut, C., Bria, M., Moreau, M., Fricoteaux, F., Miri, V., & Bacquet,
468   M. (2016). Antimicrobial citric acid/poly(vinyl alcohol) crosslinked films: Effect of cyclodextrin
469   and sodium benzoate on the antimicrobial activity. *LWT - Food Science and Technology, 68*,
470   pp. 27-35. https://doi.org/10.1016/j.lwt.2015.12.009.

471 Corvaglia, S., Rodriguez, S., Bardi, G., Torres, F. G., & Lopez, D. (2016). Chitin whiskers reinforced
472   carrageenan films as low adhesion cell substrates. *International Journal of Polymeric Materials
473   and Polymeric Biomaterials, 65*(11), pp. 574-580.
474   https://doi.org/10.1080/00914037.2016.1149846.

475 Cran, M. J., & Bigger, S. W. (2005). The effect of metallocene-catalyzed linear low-density polyethylene
476   on the physicomechanical properties of its film blends with low-density polyethylene. *Journal
477   of Materials Science, 40*(3), pp. 621-627. https://doi.org/10.1007/s10853-005-6299-4.

478 Decker, C., & Moussa, K. (1988). A new method for monitoring ultra-fast photopolymerizations by
479   real-time infra-red (RTIR) spectroscopy. *Die Makromolekulare Chemie, 189*(10), pp. 2381-
480   2394. https://doi.org/10.1002/macp.1988.021891016.

481 Delville, J., Joly, C., Dole, P., & Bliard, C. (2002). Solid state photocrosslinked starch based films: a new
482   family of homogeneous modified starches. *Carbohydrate Polymers, 49*(1), pp. 71-81.
483   https://doi.org/10.1016/S0144-8617(01)00302-2.

484 Detduangchan, N., Sridach, W., & Wittaya, T. (2014). Enhancement of the properties of biodegradable
485   rice starch films by using chemical crosslinking agents. *International Food Research Journal,
486   21*(3), pp. 1225-1235

487 El Achaby, M., Kassab, Z., Aboulkas, A., Gaillard, C., & Barakat, A. (2018). Reuse of red algae waste for
488   the production of cellulose nanocrystals and its application in polymer nanocomposites.
489   *International Journal of Biological Macromolecules, 106*, pp. 681-691.
490   https://doi.org/10.1016/j.ijbiomac.2017.08.067.

491 Farhan, A., & Hani, N. M. (2017). Characterization of edible packaging films based on semi-refined
492   kappa-carrageenan plasticized with glycerol and sorbitol. *Food Hydrocolloids, 64*, pp. 48-58.
493   https://doi.org/10.1016/j.foodhyd.2016.10.034.

Gennadios, A., Rhim, J. W., Handa, A., Weller, C. L., & Hanna, M. A. (1998). Ultraviolet Radiation Affects Physical and Molecular Properties of Soy Protein Films. *Journal of Food Science, 63*(2), pp. 225-228. https://doi.org/10.1111/j.1365-2621.1998.tb15714.x.

Kanmani, P., & Rhim, J.-W. (2014). Development and characterization of carrageenan/grapefruit seed extract composite films for active packaging. *International Journal of Biological Macromolecules, 68*, pp. 258-266. https://doi.org/10.1016/j.ijbiomac.2014.05.011.

Karbowiak, T., Ferret, E., Debeaufort, F., Voilley, A., & Cayot, P. (2011). Investigation of water transfer across thin layer biopolymer films by infrared spectroscopy. *Journal of Membrane Science, 370*(1-2), pp. 82-90. https://doi.org/10.1016/j.memsci.2010.12.037.

Khan, M. A., Bhattacharia, S. K., Kader, M. A., & Bahari, K. (2006). Preparation and characterization of ultra violet (UV) radiation cured bio-degradable films of sago starch/PVA blend. *Carbohydrate Polymers, 63*(4), pp. 500-506. https://doi.org/10.1016/j.carbpol.2005.10.019.

Kumar, A. P., & Singh, R. P. (2008). Biocomposites of cellulose reinforced starch: Improvement of properties by photo-induced crosslinking. *Bioresource Technology, 99*(18), pp. 8803-8809. https://doi.org/10.1016/j.biortech.2008.04.045.

Kuorwel, K. K., Cran, M. J., Sonneveld, K., Miltz, J., & Bigger, S. W. (2014). Physico-Mechanical Properties of Starch-Based Films Containing Naturally Derived Antimicrobial Agents. *Packaging Technology and Science, 27*(2), pp. 149-159. http://dx.doi.org/10.1002/pts.2015.

Liang, J., Wang, R., & Chen, R. (2019). The Impact of Cross-linking Mode on the Physical and Antimicrobial Properties of a Chitosan/Bacterial Cellulose Composite. *Polymers, 11*(3), pp. https://doi.org/10.3390/polym11030491.

Miranda, T. M. R., Goncalves, A. R., & Amorim, M. T. P. (2001). Ultraviolet-induced crosslinking of poly(vinyl alcohol) evaluated by principal component analysis of FTIR spectra. *Polymer International, 50*(10), pp. 1068-1072. https://doi.org/10.1002/pi.745.

Mondal, D., Bhowmick, B., Maity, D., Mollick, M. M. R., Rana, D., Rangarajan, V., Sen, R., & Chattopadhyay, D. (2015). Investigation on Sodium Benzoate Release from Poly(Butylene Adipate-Co-Terephthalate)/Organoclay/Sodium Benzoate Based Nanocomposite Film and Their Antimicrobial Activity. *Journal of Food Science, 80*(3), pp. E602-E609. https://doi.org/10.1111/1750-3841.12745.

Müller, C. M. O., Laurindo, J. B., & Yamashita, F. (2011). Effect of nanoclay incorporation method on mechanical and water vapor barrier properties of starch-based films. *Industrial Crops and Products, 33*(3), pp. 605-610. https://doi.org/10.1016/j.indcrop.2010.12.021.

Necas, J., & Bartosikova, L. (2013). Carrageenan: a review. *Veterinarni Medicina, 58*(4), pp. 187-205

Niazi, M. B. K., & Broekhuis, A. A. (2015). Surface photo-crosslinking of plasticized thermoplastic starch films. *European Polymer Journal, 64*, pp. 229-243. https://doi.org/10.1016/j.eurpolymj.2015.01.027.

Rhim, J.-W. (2013). Effect of PLA lamination on performance characteristics of agar/κ-carrageenan/clay bio-nanocomposite film. *Food Research International, 51*(2), pp. 714-722. https://doi.org/10.1016/j.foodres.2013.01.050.

Rhim, J.-W., & Wang, L. F. (2013). Mechanical and water barrier properties of agar/κ-carrageenan/konjac glucomannan ternary blend biohydrogel films. *Carbohydrate Polymers, 96*(1), pp. 71-81. https://doi.org/10.1016/j.carbpol.2013.03.083.

Salami, M., Rezaee, M., Askari, G., & Emam Djomeh, Z. (2020). UV-irradiated gelatin-chitosan bio-based composite film, physiochemical features and release properties for packaging

applications. *International Journal of Biological Macromolecules, 147*, pp. 990-996. https://doi.org/10.1016/j.ijbiomac.2019.10.066.

Sedayu, B. B., Cran, M. J., & Bigger, S. W. (2018). Characterization of Semi-refined Carrageenan-Based Film for Primary Food Packaging Purposes. *Journal of Polymers and the Environment, 26*(9), pp. 3754-3761. https://doi.org/10.1007/s10924-018-1255-y.

Sedayu, B. B., Cran, M. J., & Bigger, S. W. (2019). A Review of Property Enhancement Techniques for Carrageenan-based Films and Coatings. *Carbohydrate Polymers, 216*, pp. 287-302. https://doi.org/10.1016/j.carbpol.2019.04.021.

Sedayu, B. B., Cran, M. J., & Bigger, S. W. (2020). Improving the moisture barrier and mechanical properties of semi-refined carrageenan films. *Journal of Applied Polymer Science*, pp. early view, 49238. https://doi.org/10.1002/app.49238.

Shahbazi, M., Ahmadi, S. J., Seif, A., & Rajabzadeh, G. (2016). Carboxymethyl cellulose film modification through surface photo-crosslinking and chemical crosslinking for food packaging applications. *Food Hydrocolloids, 61*, pp. 378-389. https://doi.org/10.1016/j.foodhyd.2016.04.021.

Shankar, S., Reddy, J. P., Rhim, J.-W., & Kim, H. Y. (2015). Preparation, characterization, and antimicrobial activity of chitin nanofibrils reinforced carrageenan nanocomposite films. *Carbohydrate Polymers, 117*, pp. 468-475. https://doi.org/10.1016/j.carbpol.2014.10.010.

Sobral, P. J. A., Menegalli, F. C., Hubinger, M. D., & Roques, M. A. (2001). Mechanical, water vapor barrier and thermal properties of gelatin based edible films. *Food Hydrocolloids, 15*(4–6), pp. 423-432. https://doi.org/10.1016/S0268-005X(01)00061-3.

Sonker, A. K., Rathore, K., Nagarale, R. K., & Verma, V. (2018). Crosslinking of Polyvinyl Alcohol (PVA) and Effect of Crosslinker Shape (Aliphatic and Aromatic) Thereof. *Journal of Polymers and the Environment, 26*(5), pp. 1782-1794. https://doi.org/10.1007/s10924-017-1077-3.

Sothornvit, R., & Rodsamran, P. (2008). Effect of a mango film on quality of whole and minimally processed mangoes. *Postharvest Biology and Technology, 47*(3), pp. 407-415. https://doi.org/10.1016/j.postharvbio.2007.08.005.

Villarruel, S., Giannuzzi, L., Rivero, S., & Pinotti, A. (2015). Changes induced by UV radiation in the presence of sodium benzoate in films formulated with polyvinyl alcohol and carboxymethyl cellulose. *Materials Science and Engineering: C, 56*, pp. 545-554. http://dx.doi.org/10.1016/j.msec.2015.07.003.

Zain, A. H. M., Wahab, M. K. A., & Ismail, H. (2018). Solid-state photo-cross-linking of cassava starch: improvement properties of thermoplastic starch. *Polymer Bulletin, 75*(8), pp. 3341-3356. https://doi.org/10.1007/s00289-017-2209-6.

Zhou, J., Ma, Y., Ren, L., Tong, J., Liu, Z., & Xie, L. (2009). Preparation and characterization of surface crosslinked TPS/PVA blend films. *Carbohydrate Polymers, 76*(4), pp. 632-638. https://doi.org/10.1016/j.carbpol.2008.11.028.

Zhou, J., Zhang, J., Ma, Y., & Tong, J. (2008). Surface photo-crosslinking of corn starch sheets. *Carbohydrate Polymers, 74*(3), pp. 405-410. https://doi.org/10.1016/j.carbpol.2008.03.006.

Effects of Surface Photocrosslinking on the Properties of Semi-Refined Carrageenan Film

Bakti B. Sedayu, Marlene J. Cran, Stephen W. Bigger

Supplementary Material

Table S1. Surface color parameters of the control SRC film and SRC films crosslinked at different times of UV exposure.

UV exposure time/min	L^*	a^*	b^*	ΔE
control	86.94 ± 0.28^a	-0.01 ± 0.01^a	8.62 ± 0.42^a	12.49 ± 0.46^{ab}
5	86.93 ± 0.20^a	-0.03 ± 0.03^a	8.55 ± 0.51^a	12.46 ± 0.44^{ab}
10	86.91 ± 0.20^a	-0.11 ± 0.05^b	8.82 ± 0.39^{ab}	12.64 ± 0.37^a
20	86.97 ± 0.23^a	-0.18 ± 0.05^c	8.78 ± 0.39^{ab}	12.56 ± 0.39^{ab}
40	86.72 ± 0.24^a	-0.20 ± 0.05^c	9.20 ± 0.31^b	13.00 ± 0.36^b

Values are given as mean with a standard deviation. Any two means in the same column with a similar letter are not significantly different (p > 0.05) as determined by a Duncan test. The control sample was not treated with sodium benzoate and not exposed to UV irradiation.

Table S2. Water sensitivity and water barrier properties of the control SRC film and SRC films crosslinked at different times of UV exposure.

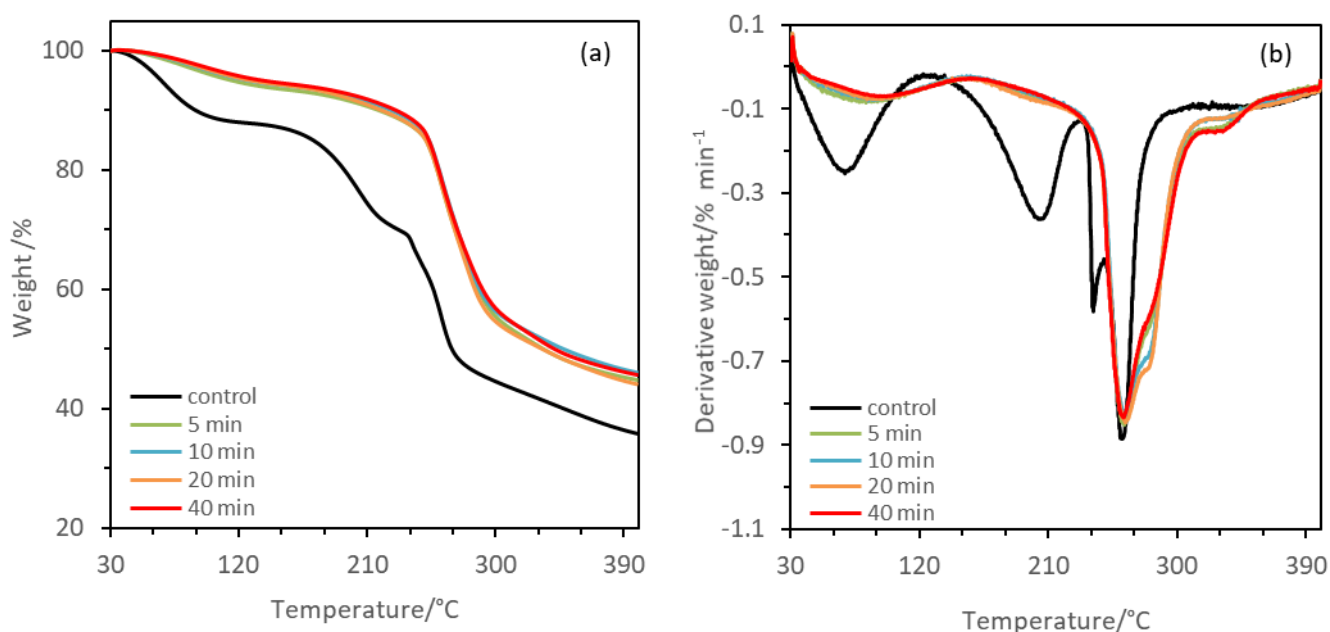| UV exposure time/min	Water content/%	Water solubility/%	Water uptake/%	Contact angle/°	WVP $\times 10^{-8}$/g mm cm^{-2} h^{-1} Pa^{-1}
control	29.81 ± 1.60^a	46.99 ± 0.37^a	37.77 ± 1.93^a	84.06 ± 3.37^a	16.4 ± 0.4^a
5	15.23 ± 0.64^b	64.52 ± 2.14^b	41.34 ± 1.56^b	65.26 ± 2.67^b	13.5 ± 0.9^{bc}
10	15.57 ± 0.22^b	65.25 ± 1.48^{bc}	44.13 ± 1.45^{bc}	66.55 ± 1.60^{bc}	13.0 ± 0.5^b
20	15.36 ± 1.06^b	67.56 ± 1.61^c	46.27 ± 1.57^c	66.67 ± 1.14^{bc}	13.9 ± 0.9^{bc}
40	13.51 ± 1.45^c	55.68 ± 1.55^d	46.10 ± 1.63^c	68.71 ± 2.07^c	14.7 ± 1.0^c

Values are given as mean with a standard deviation. Any two means in the same column with a similar letter are not significantly different (p > 0.05) as determined by a Duncan test. The control sample was not treated with sodium benzoate and not exposed to UV irradiation.

Table S3. Tensile strength, Young's modulus and elongation at break properties of the control SRC film and SRC films crosslinked at different times of UV exposure.

UV exposure time /min	Tensile strength/MPa	Young's modulus/GPa	Elongation at break/%
control	31.10 ± 1.04^a	0.484 ± 0.034^a	21.65 ± 0.97^a
5	42.20 ± 2.15^b	1.163 ± 0.041^b	10.34 ± 0.94^b
10	46.10 ± 2.97^b	1.175 ± 0.034^b	11.26 ± 0.89^{bc}
20	45.87 ± 3.05^c	1.174 ± 0.038^b	11.20 ± 0.99^c
40	43.03 ± 1.14^b	1.179 ± 0.046^b	10.65 ± 1.01^{bc}

Values are given as mean with a standard deviation. Any two means in the same column with a similar letter are not significantly different (p > 0.05) as determined by a Duncan test. The control sample was not treated with sodium benzoate and not exposed to UV irradiation.

Figure S1. Plots of: (a) normalized mass loss and (b) derivative mass loss as a function of temperature for the SRC control film and SRC films crosslinked with sodium benzoate for 5, 10, 20 and 40 min UV exposure times. Samples were heated from 30 to 400 °C at a heating rate of 10 °C min^{-1} under a nitrogen atmosphere (20 mL min^{-1} flow rate).

Figure S2. FTIR spectra of sodium benzoate, control SRC film and SRC films crosslinked for 5, 10, 20 and 40 min exposure to UV irradiation over the wavenumber ranges: (a) 3700-3000 cm^{-1}, (b) 3000-2800 cm^{-1}, (c) 1800-1300 cm^{-1}, and (d) 1300-700 cm^{-1}. Spectra are the average of 64 scans.